Accepted Manuscript

Whole-exome sequencing of acquired nevi identifies mechanisms for development and maintenance of benign neoplasms

Mitchell S. Stark, Jean-Marie Tan, Lisa Tom, Kasturee Jagirdar, Duncan Lambie, Helmut Schaider, H. Peter Soyer, Richard A. Sturm

PII: S0022-202X(18)30133-7

DOI: 10.1016/j.jid.2018.02.012

Reference: JID 1298

To appear in: *The Journal of Investigative Dermatology*

Received Date: 11 January 2018

Revised Date: 6 February 2018

Accepted Date: 13 February 2018

Please cite this article as: Stark MS, Tan J-M, Tom L, Jagirdar K, Lambie D, Schaider H, Soyer HP, Sturm RA, Whole-exome sequencing of acquired nevi identifies mechanisms for development and maintenance of benign neoplasms, *The Journal of Investigative Dermatology* (2018), doi: 10.1016/j.jid.2018.02.012.

Original article

Whole-exome sequencing of acquired nevi identifies mechanisms for development and maintenance of benign neoplasms

Mitchell S. Stark [1], Jean-Marie Tan [1], Lisa Tom [1], Kasturee Jagirdar [1], Duncan Lambie [2], Helmut Schaider [1,3], H. Peter Soyer [1,3] and Richard A. Sturm [1]

[1] Dermatology Research Centre, The University of Queensland, The University of Queensland Diamantina Institute, Translational Research Institute, Brisbane, Queensland, Australia

[2] IQ Pathology, Brisbane, Queensland, Australia

[3] Department of Dermatology, Princess Alexandra Hospital, Brisbane, Australia

Corresponding author:

Dr Mitchell S. Stark

Dermatology Research Centre,

The University of Queensland, UQ Diamantina Institute,

Level 5, Translational Research Institute,

37 Kent Street, Woolloongabba, Brisbane,

QLD 4102, Australia

Phone: +61 7 3443 8027

Fax: +61 7 3443 7779

Email: m.stark@uq.edu.au

https://orcid.org/0000-0002-4510-2161

Short Title: Whole-exome sequencing of acquired nevi

Keywords: nevi; melanoma; mutation signature; copy number; DNA repair.

Abbreviations

AMN Acquired melanocytic nevi

CNA copy number aberration

COSMIC Catalogue of somatic mutations in cancer

CPDs cyclobutane pyrimidine dimers

LOH loss-of-heterozygosity

OIS oncogene-induced senescence

SNV single-nucleotide variants

TPM *TERT* promoter mutations

UVR ultra-violet radiation

WES whole-exome sequencing

URLs

COSMIC mutation signature analysis: http://cancer.sanger.ac.uk/cosmic/signatures

ABSTRACT

The melanoma transformation rate of each nevus is rare despite the detection of oncogenic *BRAF* or *NRAS* mutations in 100% of nevi. Acquired melanocytic nevi (AMN) do however mimic melanoma and ~30% of all melanomas arise within pre-existing nevi. Using whole-exome sequencing of 30 matched nevi, adjacent normal skin, and saliva we sought to identify the underlying genetic mechanisms for nevus development. All nevi were clinically, dermoscopically, and histopathologically documented. In addition to identifying somatic mutations, we found mutational signatures relating to ultra-violet radiation (UVR) mirroring those found in cutaneous melanoma. In nevi we frequently observed the presence of the UVR mutation signature compared to adjacent normal skin (97% vs 10% respectively). In copy number aberration (CNA) analysis, in nevi with copy number loss of tumor suppressor genes (TSG), these were balanced by loss of potent oncogenes. Moreover, reticular and non-specific patterned nevi revealed an increased ($p<0.0001$) number of CNA as compared with globular nevi. The mutation signature data generated in this study confirms that UVR strongly contributes to nevogenesis. Copy number changes reflect at a genomic level the dermoscopic differences of AMN. Lastly, we propose that the balanced loss of TSGs and oncogenes is a protective mechanism of AMN.

INTRODUCTION

Melanocytic nevi are acquired benign neoplasms of the skin derived from melanocytes. In both children and adults, new nevi can form and existing ones change regularly (Abbott et al., 2014, Duffy et al., 2004, Menzies et al., 2011) which can be closely monitored for diagnostic purposes in melanoma screening. Many benign melanocytic lesions are excised unnecessarily as most nevi, even with a change in morphology, will never develop into a melanoma. Despite the rarity of transformation of an individual nevus (Tsao et al., 2003), it has been reported that ~30% (range; 4-72%) of melanoma have arisen from a pre-existing nevus (Pampena et al., 2017) hence the reasoning for close monitoring. Indeed, Shain *et al.* (Shain et al., 2015) showed that in archival clinical specimens, which had a melanoma adjacent to a nevus, that there were many shared mutations and copy number aberrations consistent with a linear pathway from melanocyte to transformed precursor to melanoma. However, the conundrum still exists in that ~70% of melanomas arise *de novo* (Pampena et al., 2017) without any histopathological evidence for a precursor lesion. Improving the understanding of nevus development and transformation is therefore the key to understanding the etiology of melanoma and more efficient prevention and early detection methods for this increasingly common malignancy.

RESULTS AND DISCUSSION

Study sample and somatic mutation burden in nevi

Using whole-exome sequencing (WES) we assessed the somatic mutational landscape, mutation signatures and copy-number aberrations (CNA) in 30 acquired pigmented melanocytic nevi and matching adjacent normal skin (perilesional). The prospectively collected nevi were classified clinically as having a globular (n=12) or reticular/non-specific (n=18) pattern and were histopathologically diagnosed (DL) as benign/dysplastic lesions with common architectural features (**Table S1**). Somatic single-nucleotide variants (SNVs) were identified in all nevi lesional tissue from the exome pull-down region (coding and untranslated regions) with ranges from 30-668 mutations (median, 256) or 0-9 mutations per megabase (muts/Mb). The total number of deleterious mutations (nonsense and nonsynonymous) ranged from 13-340 SNVs (median, 89) which is higher than those previously described in a study of 19 dysplastic nevi (range 0-46; median, 19) (Melamed et al., 2017). The observed differences are likely due to the sample populations with all of our nevi derived from a population that have a history of frequent sun exposure combined with a geographical region that has one of the highest level of UVR in the world (Brisbane, Australia).

Somatic single-nucleotide variant subclasses in nevi and matching perilesional skin

Not surprisingly, C>T transitions were confirmed to be the most prevalent SNV class (**Fig. 1a)** and subsequent investigation into the tri-nucleotide context (e.g. N[C>T]N) showed that overall the nevi analysed here share many similarities to the mutation frequency distribution in cutaneous melanoma (see Materials and Methods) (**Fig. 1b**). The point of difference between nevi and melanomas can be seen with the ratio of T[C>T]G:T[C>T]C being higher in melanoma (**Fig. 1b**). Interestingly, this increase in T[C>T]G transitions corresponds to the

presence of deleterious mutations in tumor suppressor genes such as *ARID2, ATM, DCC,* and *NF1*; all of which are absent in our nevi and in nevi analysed by Melamed et al (Melamed et al., 2017). This supports the notion that loss of tumor suppressor gene function contributes to melanomagenesis.

In matching perilesional skin, C>T transitions were again the most prevalent (**Fig. 1c**) yet this did not match the mutation profile observed in nevi (**Fig. 1d-e**). Given the proportion of C>T SNVs accounts for the majority of the variants observed, we next chose to focus on these variant types. When dermoscopic patterns were compared, globular nevi had a significantly (p=0.013) higher proportion of T[C>T]A transitions *cf.* reticular/non-specific nevi (**Fig. 2a).** When histopathologic were compared, it was revealed that intradermal nevi had a significantly increased amount of G[C>T]C and T[C>T]A variants (p=0.03 and p=0.04 respectively) *cf.* junctional/compound nevi (**Fig. 2b)** (see **Table S1** for corresponding details). These data indicate that the differences observed in the dermoscopic patterns can be related to their histopathological classification with the globular nevi in our dataset having primarily a dermal component. Importantly, there were no significant differences in C>T transitions in dysplastic *cf.* benign nevi which suggests that the broad and non-specific classification of 'dysplastic' nevi is inaccurate. Overall, these data suggest that specific mutation types may contribute to the development of distinct dermoscopic and histopathologic nevus phenotypes.

Driver gene analysis in nevi

Previous studies have used a targeted gene approach to identify likely 'driver' genes in amongst a sea of 'passenger' genes (Cheng et al., 2015, Shain et al., 2015). Using a combined gene list from these studies, the number of driver genes that harboured a deleterious mutation present in our nevi ranged from 1-14 (**Table S2**). Mutually exclusive

mutations in *BRAF* and *NRAS* were the most frequent (83% and 17% respectively) which is in keeping with our prior study using droplet digital PCR (Tan et al., 2018). Other genes of note included *MET* with three mutations (10%; NM_000245: Glu266Lys, Pro712Thr, and Gly1151Arg), and *GRIN2A* with two mutations (7%; NM_000833: Arg899Trp and Pro1132Leu). Targeted gene panels allow for a focused approach but are limited to identifying known genes. In addition to these well-known genes, we identified genes such as *HDAC9* (NM_058176: p.Ser612Phe), *MYH11* (NM_002474:p.Gly743Glu), and *DCC* (NM_005215: p.Asp866Asn) which were flagged as predicted driver mutations using IntOGen (Gonzalez-Perez et al., 2013) (**Table S3**). Interestingly these 'driver' mutations are present at a similar variant allele frequency as $BRAF^{V600E}$ and $BRAF^{V600K}$ respectively which indicate that they most likely occurred at the same time during nevus formation. Notably, *BRAF* mutations have been observed to occur in all cells present in a nevus, as such nevi are considered to be clonal, originating from a single initiated melanocyte (Yeh et al., 2013). However alternative to this, is the theory that nevi are not always clonal but can be polyclonal (Lin et al., 2009). In our study, we find evidence for both notions (**Table S2)** although in most cases where a *BRAF* mutation appears in a 'clonal' nevus, other gene mutations co-occur at a similar mutation frequency as noted (**Tables S2 and S3)**. In cases where *BRAF* mutations occur at a sub-clonal frequency (< % nevus cell estimate), it is unclear if this is due to a late acquisition of the *BRAF* mutation or an observation of oncogene-induced senescence (OIS) (Michaloglou et al., 2005) in the initial nevus cell population followed by an outgrowth of cells that have acquired a selective advantage via a new mutation. Given that *BRAF* V600 mutations are the most prevalent, they are likely to be the initiator and the other genes contain private deleterious mutations that provide a permissive environment for nevus development.

TERT promoter mutation analysis in nevi

TERT promoter mutations (TPM) are prevalent in melanoma (60-86%) (Cancer Genome Atlas, 2015, Hayward et al., 2017, Horn et al., 2013, Huang et al., 2013) and have also been observed in 'intermediate' melanocytic lesions (Shain et al., 2015) that occur adjacent to a melanoma. We did not detect any of the common TPMs (data not shown) in our benign or dysplastic lesions which was not an unexpected finding considering there was no evidence for malignant transformation observed clinically or histopathologically.

Mutation signature analysis in nevi and matching perilesional skin

The underlying causative mechanisms for most of the common malignancies investigated to date can be elucidated by analysing somatic mutation signatures (Alexandrov et al., 2013). Each unique signature is named "signature 1-30" and is defined by the pattern and proportion of specific trinucleotides present in each sample (see COSMIC mutation signature URL for definitions). In cutaneous melanoma, it has been established that UVR creates a well-known somatic mutation signature ("signature 7"). We confirm that the predominance of C>T transitions observed in our nevi resulted in a prevalent proportion of signature 7 related SNVs (97% or 29/30; range 0-82%, median 61%; **Fig. 3a** and **Table S4**). Three of the 30 nevi (10%) had a low signature 7 proportion (0-13%; **Tables S1 and S4**) which correlated with no or limited UVR exposure based upon body location and clinical evidence of sun exposure. This suggests that acquired melanocytic nevi are not always initiated via UVR exposure. An age-related signature (signature 1) (Alexandrov et al., 2013) was the next most prevalent (93% or 28/30; range 0-61%, median 26%; **Fig. 3a** and **Table S4**). However we could find no significant association with signature 1 with age at lesion excision (data not shown). Remarkably, two samples had no signature 1 along with a low or absent signature 7 (13% and 0% respectively). Instead of these common signatures, evidence for defective DNA mismatch repair (Alexandrov et al., 2013) was identified (signature 20; 23% and signature 6, 13% respectively). This highlights an alternative mechanism for nevi development in the absence

of UVR. Defects in DNA repair is in fact prevalent in our nevi (10/30 or 33%) with many mutually exclusive signatures being identified (signatures 3, 6, 15, 20, and 26) (Alexandrov et al., 2013) (**Fig. 3a and Table S1 and S4)** which confirms that defective DNA repair contributes to nevogenesis.

Recent studies have established that sun-exposed skin derived from the eyelid have an excess of C>T mutations in a targeted panel of genes (Martincorena et al., 2015). Using WES we were able to determine the somatic mutations present in 30 matching normal skin samples (**Table S5**). We too observed a predominance of C>T mutations, however surprisingly this did not culminate into a UVR signature in all samples (10% or 3/30; **Fig. 3b**). Defective DNA repair signatures (signatures 3 and 26) (Alexandrov et al., 2013) were however frequently observed (83% and 50% respectively) along with signature 1 (100%).

These mutation signature data suggest a number of scenarios. Firstly, the accumulation of age-related mutations and defective DNA repair machinery, lead to the accumulation of UVR signature mutations in a given melanocyte, which contributes to nevogenesis. Secondly, the absence of the classical UVR signature mutations in the perilesional skin which predominates in the more pigmented (and thus more melanin containing) nevi, suggests that the melanin content may contribute to the excess of C>T transitions specific to the UVR signature. This notion is supported by the study by Premi *et al.* (Premi et al., 2015) which described that the many of cyclobutane pyrimidine dimers (CPDs) arise via the breakdown of melanin pigment.

Somatic mutation type and mutation signature analysis of nevi relative to body location/degree of sun exposure

Next we investigated nevi located on different body sites in combination with clinical evidence of sun exposure. Indeed, nevi located on ‘shielded’ sites (**Table S1**) were significantly (p=0.006) more likely to have a higher proportion of insertion/deletions (indels)

(**Fig. 4a**) as compared with nevi located on 'sun exposed' sites which were more likely (p=0.03) to have a higher proportion of deleterious mutations. Not surprisingly, nevi from sun-exposed sites had a higher proportion of signature 7 mutations (p=0.001) (**Fig. 4a**) which is consistent with UVR contributing to high somatic mutation burden. Moreover, in nevi that had a signature 7 profile that was less than the observed median (61%); these nevi were more likely (p=0.014) to have a defective DNA repair signature (**Fig. 4b**) which in turn was more likely (p=0.045) to be present in dysplastic nevi (**Fig. 4c**). Interestingly, there was no significant differences (data not shown) in the different dermoscopic patterned nevi based on degree of body site/sun exposure, the proportion of signature 7 or DNA repair defect signatures, or the proportion of deleterious mutations present. However reticular/non-specific nevi where more likely (p=0.002) to have a higher proportion of indels (**Fig 4d**) *cf*. globular nevi which may suggest an alternative mechanism for development.

Copy number aberration analysis of nevi

In addition to high somatic mutation burden, cutaneous melanomas have an increased amount of copy number aberrations (CNA). Specifically, melanomas often have focal deletions in tumor suppressor genes (e.g. CDK2NA), focal amplifications in oncogenes (e.g. *MITF*), along with extensive regions of copy number loss-of-heterozygosity (LOH) often encompassing whole chromosomal arms (Stark and Hayward, 2007). Complex genomic rearrangements are also the hallmark of non-UVR induced mucosal and acral melanomas (Hayward et al., 2017). Interestingly, our dermoscopically globular nevi were largely genomically silent with minor CNAs observed (**Fig. 5a**), however in stark contrast we detected a high frequency of genome-wide CNAs in our reticular/non-specific nevi (p<0.0001; **Fig 5b; Table S6-7**) which correlates with the higher proportion of observed indels. Considering the extensive nature of the CNAs present in the reticular/non-specific nevi, one would assume that this may herald the early beginnings of a melanoma. However,

upon closer inspection of the genes involved, the CNAs appear to be balanced events. Importantly, the majority of the observed CNAs were large regional CNAs (mainly LOH) rather than focal regions of loss which is a hallmark of cutaneous melanoma. These large regional events suggest that no specific gene is being targeted; instead this is a random mutagenic process. To find evidence for LOH events effecting gene expression, interrogation of the melanoma TCGA data (Cancer Genome Atlas, 2015) revealed that on average, LOH of key melanoma genes can significantly result in a loss of expression in tumor suppressors as well as in oncogenes (**Fig. S1 and S2**). We therefore postulate that the net effect of the loss of both gene functions in the same nevus specimen combine to have an overall copy neutral effect, thus keeping the nevus in a state of equilibrium so as to be 'protected' against malignant transformation.

In summary, this study has highlighted that acquired nevi occur in most cases following cumulative exposure to UVR together with defective DNA repair mechanisms in normal skin melanocytes. This environment permits the accumulation of UV-related somatic mutations which is evident in the mutation signatures (**Table S1**, **S4**, and **Figure 6**) observed in our nevi and matching adjacent skin. Moreover, we predict that CNA events that are balanced (or absent) in clonally expanded melanocytes, lead to the nevogenesis pathway. Lastly, if these CNA events become imbalanced in a given clonal expansion, then this contributes to the formation of early melanomas.

MATERIALS AND METHODS

Patients and tissue sampling

This study was approved by the Metro South Human Research Ethics Committee (Brisbane, Australia; HREC/09/QPAH/162) and was carried out in accordance with the Declaration of Helsinki. With written informed consent, 30 acquired melanocytic nevi with the globular (n=12), reticular (n=14) and non-specific (n=4) dermoscopic patterns identified by a board certified dermatologist (HPS) from a database of prospectively imaged nevi (Daley et al., 2016) were excised by shave excision from 20 participants. Of these 10 donated a single nevus and the following 10 participants had two nevi excised: 07LW, 28RH, 111CM, 158RP, 61JB, 510AN, 673PS, 736TP, 822MT, and 1346KJ, (**Table S1**). Each nevus was bisected and one half of the tissue was formalin-fixed and histopathologically diagnosed by a board certified pathologist (DL). The second half of the tissue was dissected to isolate nevus from adjacent perilesional skin according to methods previously described (Tan et al., 2018). DNA extraction was performed as described previously (Tan et al., 2018). Saliva was collected and germline DNA was extracted from each study participant as previously described (Daley et al., 2016).

Somatic variant calling and filtering

Somatic variants present in the nevi and perilesional samples were determined firstly by filtering out all variants that were present in the matching saliva-derived germline DNA followed by all variants that were present in 1000g2014oct_eur and ExAC NFE databases. Variants present in dbSNP 138 were not used as a filter due to the presence of somatic mutations (eg. $BRAF^{V600E}$). Accordingly, a proportion of the variants presented in **Tables S3 and S5** may indeed be polymorphisms. Next, any variant present in a pool of 30 perilesional samples were removed from each the nevi samples which resulted in a list of somatic variants

present only in the lesion and not from perilesional contamination. Next, all somatic variants present in the nevi and perilesion were filtered further to include only those with a total of ≥10 reads, an alternative read frequency of ~3% (based upon known a mutation in $NRAS^{Q61K}$ previously determined by ddPCR (Tan et al., 2018)), a variant $p \leq 0.05$, and an alternate Phred base quality of 30.

Detection of known mutations

In order to test the sensitivity of the exome sequencing depth for identifying somatic mutations in *BRAF* or *NRAS* present in our nevi samples (Tan et al., 2018), we first used The Integrative Genome Viewer (IGV, Broad Institute) to visualise the BAM files at specific codons. *BRAF* V600E/K mutations were detectable in all samples (26/26; **Table S2**) and *NRAS* G13C and Q61L/K/R were detectable in the remaining 4/4 samples (**Table S2**). The digital PCR methodology employed in our prior study (Tan et al., 2018) detected additional *NRAS* G13C mutations in samples with codon 61 mutations which were not detectable in our exome dataset as they were less than the limit of detection (~1% mutant frequency). Furthermore, the *NRAS* Q61L mutation detected in 903JA-33 via exome sequencing was not validated using ddPCR and instead was found to have an *NRAS* G13C mutation. The *NRAS* Q61L is possibly a false positive result. Next, we confirmed the presence of the validated mutations in the stringently filtered dataset as described. *BRAF*/*NRAS* mutations were detectable in 17/30 samples with 13/30 not passing filtering due to low mutant allele frequency (10/13) and were filtered out during variant calling; or the mutant call had a $p>0.05$ (3/13) as determined via VarScan2 (Koboldt et al., 2012).

TERT promoter sequence analysis

The *TERT* promoter region was amplified using forward (5'-ACGAACGTGGCCAGCGGCAG-3') and reverse (5'- CTCCCAGTGGATTCGCGGGC-3')

primer sequences designed using Primer3web (v4.0.0) software. To increase the specificity of the primers, a touchdown PCR protocol was employed with a cycling routine of two cycles at each annealing temperature commencing at 69°C, decreasing by 1°C steps (69°C-63°C), followed by 20 cycles at the optimal temperature (62°C). All other cycling conditions were as per manufacturers protocol (Thermo Fisher Scientific). PCR reactions consisted of 25-50ng of DNA, 0.5µM of each primer, 200µM dNTPs (Thermo Fisher Scientific), together with 0.4U of Phusion Hot start II High-Fidelity DNA polymerase (#F-549, Thermo Fisher Scientific), 5X Phusion GC buffer (supplemented with $MgCl_2$; #F-519) and 5% DMSO. The 369bp PCR products were electrophoresed on a 2% TAE agarose gel, purified using the QIAquick Gel Extraction Kit (QIAGEN), then sequenced using the BigDye™ Terminator v3.1 Cycle Sequencing Kit (Thermo Fisher Scientific) as per manufacturer's instructions. Agencourt CleanSEQ (Beckman Coulter Life Sciences) purified products were run on the 3730-series Genetic Analyzer (Thermo Fisher Scientific) by the Australian Equine Genetics Research Centre (AEGRC, Brisbane, Australia). All *TERT* promoter sequence chromatograms were analyzed using Sequencher 5.4 software (Gene Codes Corporation) in comparison with hg19 reference sequence (chr5: 1,295,022-1,295,495).

Mutation signature analysis

Filtered somatic SNVs present in the nevi and perilesional skin were imported into the deconstructSigs (Rosenthal et al., 2016) package using R 3.4.0 for Windows (https://github.com/raerose01/deconstructSigs). Mutation signatures were determined by using the framework of 30 Cosmic signatures (http://cancer.sanger.ac.uk/cosmic/signatures) collated in the deconstructSigs package. Somatic mutations present in melanoma datasets were downloaded from ftp://ftp.sanger.ac.uk/pub/cancer/AlexandrovEtAl/somatic_mutation_data/Melanoma/ and imported into the deconstructSigs package as described.

Copy Number Analysis

Copy number aberrations were determined via the CNVkit (Rieber et al., 2017) package (https://github.com/etal/cnvkit) and run using Python 2.7. Briefly, matching nevi and perilesion BAM files, with duplicates marked and sorted (see methods above) where analysed within CNVkit according to standard methods. The matching perilesion was used as the background normal. Nevus cell content was estimated based upon *BRAF* mutation frequency as determined by methods previously reported (Shain et al., 2015). In the absence of *BRAF* mutation, tumor cell fraction was estimated from H&E sections by an experienced dermatopathologist (HPS). A segmentation file (**Table S6**) was compiled from all lesions to allow for genome-wide visualisation (**Figure 5**) in the IGV. Genes involved in regions of gain (log2 ≥3) and loss (log2 ≤-1) summarised in **Table 1**, were those commonly mutated in melanoma (Cancer Genome Atlas, 2015). The effect of copy number on RNA expression in exemplar genes derived from **Table 1** and shown in **Supplementary Figures 1 and 2** was determined using the melanoma TCGA datasets accessed via the cBioPortal for Cancer Genomics (http://www.cbioportal.org/) (Cerami et al., 2012, Gao et al., 2013).

Statistical Analysis

Box plots and statistical analysis and was performed using 2-tailed *t-tests* (Mann-Whitney), or Fisher's exact test with GraphPad Prism version 7.03 for Windows (La Jolla, California, USA) or SPSS Statistics v.24 (IBM, USA). A *p*-value <0.05 was considered statistically significant.

CONFLICTS OF INTEREST

The authors state no conflict of interest.

ACKNOWLEDGMENTS

The authors would like to thank the study participants, and are grateful for support of their colleagues particularly Katie Lee and Clare Primiero. This work was funded by project grants (APP1062935, APP1083612), and the Centre of Research Excellence for the Study of Nevi (APP1099021) from the National Health and Medical Research Council (NHMRC), Australia; and the Merchant Charitable Foundation. JMT holds a scholarship from the Australian Government Department of Education and Training. RAS and MSS hold fellowships (APP1043187 and APP1106491 respectively) from the NHMRC.

REFERENCES

Abbott NC, Pandeya N, Ong N, McClenahan P, Smithers BM, Green A, et al. Changeable naevi in people at high risk for melanoma. The Australasian journal of dermatology 2014.

Alexandrov LB, Nik-Zainal S, Wedge DC, Aparicio SA, Behjati S, Biankin AV, et al. Signatures of mutational processes in human cancer. Nature 2013;500(7463):415-21.

Cancer Genome Atlas N. Genomic Classification of Cutaneous Melanoma. Cell 2015;161(7):1681-96.

Cerami E, Gao J, Dogrusoz U, Gross BE, Sumer SO, Aksoy BA, et al. The cBio cancer genomics portal: an open platform for exploring multidimensional cancer genomics data. Cancer Discov 2012;2(5):401-4.

Cheng DT, Mitchell TN, Zehir A, Shah RH, Benayed R, Syed A, et al. Memorial Sloan Kettering-Integrated Mutation Profiling of Actionable Cancer Targets (MSK-IMPACT): A Hybridization Capture-Based Next-Generation Sequencing Clinical Assay for Solid Tumor Molecular Oncology. J Mol Diagn 2015;17(3):251-64.

Daley GM, Duffy DL, Pflugfelder A, Jagirdar K, Lee KJ, Yong XL, et al. GSTP1 does not modify MC1R effects on melanoma risk. Exp Dermatol 2016.

Duffy DL, Box NF, Chen W, Palmer JS, Montgomery GW, James MR, et al. Interactive effects of MC1R and OCA2 on melanoma risk phenotypes. Hum Mol Genet 2004;13(4):447-61.

Gao J, Aksoy BA, Dogrusoz U, Dresdner G, Gross B, Sumer SO, et al. Integrative analysis of complex cancer genomics and clinical profiles using the cBioPortal. Science signaling 2013;6(269):pl1.

Gonzalez-Perez A, Perez-Llamas C, Deu-Pons J, Tamborero D, Schroeder MP, Jene-Sanz A, et al. IntOGen-mutations identifies cancer drivers across tumor types. Nat Methods 2013;10(11):1081-2.

Hayward NK, Wilmott JS, Waddell N, Johansson PA, Field MA, Nones K, et al. Whole-genome landscapes of major melanoma subtypes. Nature 2017;545(7653):175-80.

Horn S, Figl A, Rachakonda PS, Fischer C, Sucker A, Gast A, et al. TERT promoter mutations in familial and sporadic melanoma. Science 2013;339(6122):959-61.

Huang FW, Hodis E, Xu MJ, Kryukov GV, Chin L, Garraway LA. Highly recurrent TERT promoter mutations in human melanoma. Science 2013;339(6122):957-9.

Koboldt DC, Zhang Q, Larson DE, Shen D, McLellan MD, Lin L, et al. VarScan 2: somatic mutation and copy number alteration discovery in cancer by exome sequencing. Genome Res 2012;22(3):568-76.

Lin J, Takata M, Murata H, Goto Y, Kido K, Ferrone S, et al. Polyclonality of BRAF mutations in acquired melanocytic nevi. J Natl Cancer Inst 2009;101(20):1423-7.

Martincorena I, Roshan A, Gerstung M, Ellis P, Van Loo P, McLaren S, et al. Tumor evolution. High burden and pervasive positive selection of somatic mutations in normal human skin. Science 2015;348(6237):880-6.

Melamed RD, Aydin IT, Rajan GS, Phelps R, Silvers DN, Emmett KJ, et al. Genomic Characterization of Dysplastic Nevi Unveils Implications for Diagnosis of Melanoma. J Invest Dermatol 2017;137(4):905-9.

Menzies SW, Stevenson ML, Altamura D, Byth K. Variables predicting change in benign melanocytic nevi undergoing short-term dermoscopic imaging. Arch Dermatol 2011;147(6):655-9.

Michaloglou C, Vredeveld LC, Soengas MS, Denoyelle C, Kuilman T, van der Horst CM, et al. BRAFE600-associated senescence-like cell cycle arrest of human naevi. Nature 2005;436(7051):720-4.

Pampena R, Kyrgidis A, Lallas A, Moscarella E, Argenziano G, Longo C. A meta-analysis of nevus-associated melanoma: Prevalence and practical implications. J Am Acad Dermatol 2017.

Premi S, Wallisch S, Mano CM, Weiner AB, Bacchiocchi A, Wakamatsu K, et al. Photochemistry. Chemiexcitation of melanin derivatives induces DNA photoproducts long after UV exposure. Science 2015;347(6224):842-7.

Rieber N, Bohnert R, Ziehm U, Jansen G. Reliability of algorithmic somatic copy number alteration detection from targeted capture data. Bioinformatics 2017.

Rosenthal R, McGranahan N, Herrero J, Taylor BS, Swanton C. DeconstructSigs: delineating mutational processes in single tumors distinguishes DNA repair deficiencies and patterns of carcinoma evolution. Genome Biol 2016;17:31.

Shain AH, Yeh I, Kovalyshyn I, Sriharan A, Talevich E, Gagnon A, et al. The Genetic Evolution of Melanoma from Precursor Lesions. N Engl J Med 2015;373(20):1926-36.

Stark M, Hayward N. Genome-wide loss of heterozygosity and copy number analysis in melanoma using high-density single-nucleotide polymorphism arrays. Cancer Res 2007;67(6):2632-42.

Tan JM, Tom LN, Jagirdar K, Lambie D, Schaider H, Sturm RA, et al. The BRAF and NRAS mutation prevalence in dermoscopic subtypes of acquired naevi reveals constitutive mitogen-activated protein kinase pathway activation. Br J Dermatol 2018;178(1):191-7.

Tsao H, Bevona C, Goggins W, Quinn T. The transformation rate of moles (melanocytic nevi) into cutaneous melanoma: a population-based estimate. Arch Dermatol 2003;139(3):282-8.

Yeh I, von Deimling A, Bastian BC. Clonal BRAF mutations in melanocytic nevi and initiating role of BRAF in melanocytic neoplasia. J Natl Cancer Inst 2013;105(12):917-9.

FIGURE LEGENDS

Figure 1: Single nucleotide variants (SNV) present in nevi and matching adjacent skin compared to cutaneous melanoma

(a) Box and whisker plots (5-95th percentile) of the percentage of the 6 SNV classes (C>A, C>G, C>T, T>A, T>C, and T>G) somatically observed in melanocytic nevi (n=30). **(b)** Bar graph of the median C>T trinucleotide context[#] proportion observed in melanocytic nevi (n=30) is highly correlative with those observed in cutaneous melanoma (n=396). **(c)** Box and whisker plots (5-95th percentile) of the percentage of the 6 SNV classes somatically observed in perilesional skin samples (adjacent to melanocytic nevi) (n=30). **(d)** Bar graph of the median C>T trinucleotide context proportion observed in perilesional skin samples (n=30) highlighting the low correlation compared with nevi and melanoma **(b)**. **(e)** Bar graph of the median 96 trinucleotide mutation profile observed in nevi (n=30) and matching perilesional skin (n=30).

[#] T[C>T]G is an example of a C>T trinucleotide context which can alternatively be written as TCG>TTG

Figure 2: The trinucleotide context of C>T SNVs in different dermoscopic and histopathological subtypes of nevi

Box and whisker plots (min to max) of the percentage of C>T variant types that reached statistical significance (p<0.05) when dermoscopic and histotype subtypes of nevi were compared (Mann-Whitney U-test). (**a)** Nevi classified as globular have a significantly (p=0.0132) higher proportion of T[C>T]A transitions *cf.* reticular/non-specific nevi and (**b)** intradermal nevi have a significantly increased amount of G[C>T]C and T[C>T]A variants (p=0.03 and p=0.04 respectively) *cf.* junctional/compound nevi. *P* values are indicated on graphs.

Figure 3: Mutation signatures present nevi and matching adjacent skin

Box and whisker plots (5-95th percentile) of the percentage of the common COSMIC mutation signatures (n=30) present in our **(a)** nevi (n=30) and **(b)** matching perilesional skin (n=30). For description of COSMIC mutation signatures please refer to the URL http://cancer.sanger.ac.uk/cosmic/signatures.

Figure 4: Somatic mutation type and mutation signature of nevi relative to body location/degree of sun exposure

(a) Insertion deletion mutations are more commonly found in sun-shielded nevi (p=0.0062) and sun exposed nevi are more likely to have deleterious mutations (p=0.03) and a higher proportion of signature 7 mutations (p=0.0013). **(b)** The total number of nevi that have a signature 7 mutation profile < the median (61%) are more likely to have defective DNA repair signatures present (p=0.0142). **(c)** Dysplastic nevi are more likely to have a defective DNA repair signatures (p=0.045) present while there are no significant differences in signature 7 mutations relative to benign nevi. **(d)** Reticular/non-specific patterned nevi are more likely to have an insertion deletion mutation (p=0.0017) whilst there is no significant difference in deleterious mutations between dermoscopic subtypes. *P* values are indicated on graphs. ns = p>0.05.

Figure 5: Copy number aberrations in different dermoscopic patterned nevi

Genome-wide copy number aberrations (CNAs) in dermoscopic patterned **(a)** globular and **(b)** reticular/non-specific nevi. Globular nevi are largely genomically silent with minor CNAs observed **(a)** and reticular/non-specific nevi have significantly (p<0.0001) more CNAs with mostly large regional LOH events being present. Chromosomes are represented from left to right in chromosomal order. Dark blue = copy number equivalent to homozygous deletion (HD or deep deletion); Light blue = copy number equivalent to loss of heterozygosity (LOH

or shallow deletion); Light red = copy number equivalent to 3 copies (gain); and Dark red = copy number equivalent to >3 copies (amplified).

Figure 6: Model for the fate of clonally expanded skin melanocytes

Somatic mutation signature and copy number aberration (CNA) analysis allows for insights into nevogenesis. This model shows that normal skin melanocytes accumulate mutations if there are defects in normal DNA-repair mechanisms. Over time, clonal expansion occurs and in most cases forms a benign nevus which has balanced CNA events thereby protected against malignant transformation. If imbalanced CNA events occur, then the clonally expanded melanocytes follow the melanomagenesis pathway. Melanoma can directly arise from a benign nevus or via the intermediate neoplasm state.

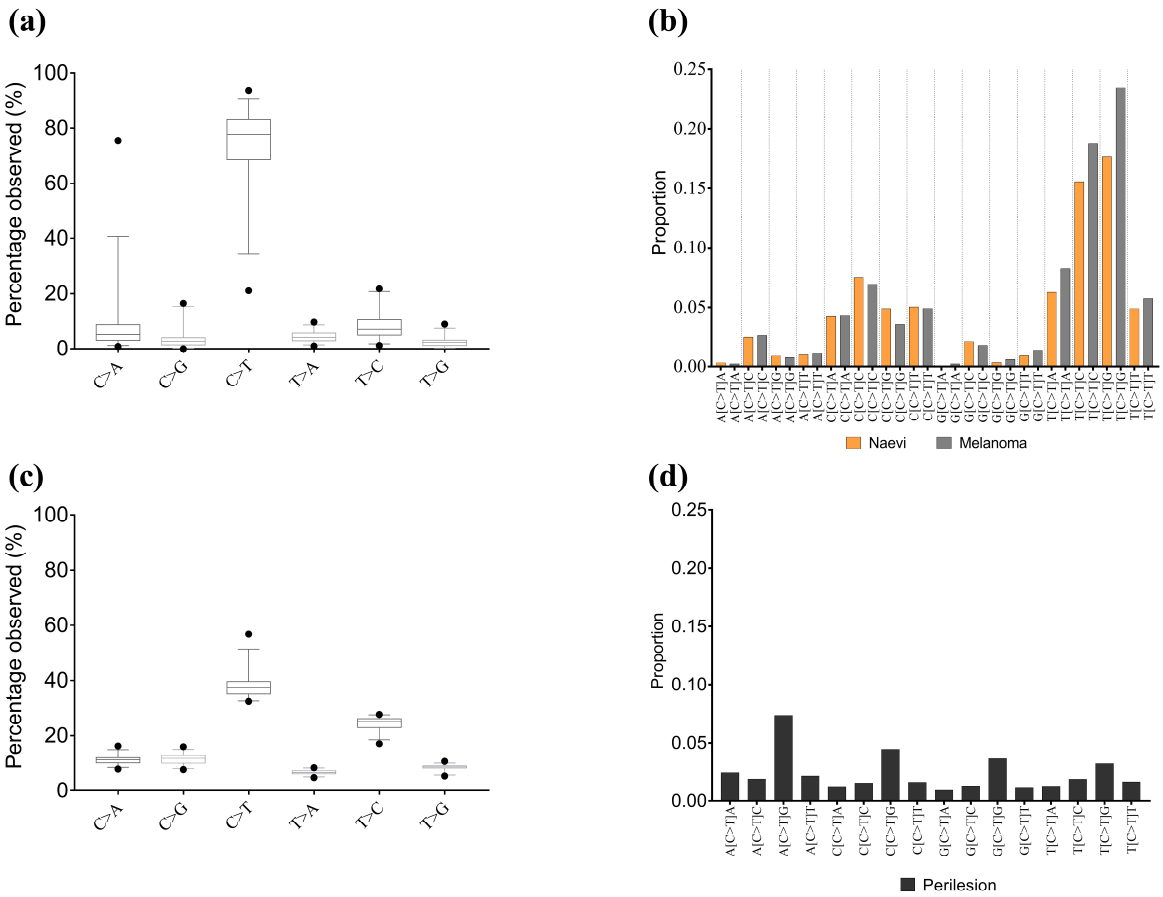
(a)
Percentage observed (%)
100
80
60
40
20
0
C>A
C>G
C>T
T>A
T>C
T>G
(b)
Proportion
0.25
0.20
0.15
0.10
0.05
0.00
Naevi
Melanoma
(c)
Percentage observed (%)
100
80
60
40
20
0
C>A
C>G
C>T
T>A
T>C
T>G
(d)
Proportion
0.25
0.20
0.15
0.10
0.05
0.00
Perilesion